This is a postprint of: Progress in Organic Coatings 99 (2016) 11-22

CORROSION BEHAVIOUR OF COATED STEEL REBARS IN CARBONATED AND CHLORIDE CONTAMINATED ALKALI-ACTIVATED FLY ASH MORTARS

M. Criado[1,2*], I. Sobrados[1], J. M. Bastidas[3], J. Sanz[1]

[1] Materials Science Institute of Madrid (ICMM), CSIC, Sor Juana Inés de la Cruz 3, 28049 Cantoblanco-Madrid, Spain

[2] Department of Materials Science and Engineering, The University of Sheffield, Sir Robert Hadfield Building, Sheffield S1 3JD, UK

[3] National Centre for Metallurgical Research (CENIM), CSIC, Avda. Gregorio del Amo 8, 28040 Madrid, Spain

ABSTRACT

The corrosion behaviour of hybrid organic-inorganic coatings of carbon steel embedded in carbonated and chloride contaminated ordinary Portland cement (OPC) and alkali-activated fly ash (AAFA) mortars was evaluated using electrochemical techniques. Sol-gel coatings were prepared by condensation and polymerization of TEOS/MPTS, TEOS/MTES, TMOS/MPTS and TMOS/MTES mixtures with a molar ratio of 1.0, and deposited by dip-coating on the carbon steel substrates. The coated steels embedded in AAFA mortars presented higher corrosion potential and lower corrosion current density values than the OPC mortars, indicating that the coatings were more efficient in preventing the corrosion of the rebars when embedded in AAFA cementitious systems. Particularly, the hybrid coatings synthesized with TEOS/MTES and TMOS/MTES mixtures showed the longest permanence of steel in the passive state,

when covering rebars embedded in carbonated AAFA mortars. This enhancement of the protection may be due to a denser and compact structure of the hybrid coatings and a greater adhesion to the metallic surface.

Keywords: Hybrid organic-inorganic coatings; Alkali activated cement; Corrosion; Carbonation; Chloride; Electrochemical techniques

* Corresponding Author: m.criado@sheffield.ac.uk (M. Criado), Phone +44 114 222 4261, Fax +44 114 222 5943

1 INTRODUCTION

Concrete is the most widely used construction material in the world, whose current consumption is estimated to be 1 m^3 per person per year [1]. The cement industry is regarded to be responsible for up to 6−7% of all the greenhouse gases emitted world-wide, with a production of 0.85−1.0 tonnes of carbon dioxide (CO_2) per ton of cement. This is mainly a consequence of (i) calcination of limestone, one of the key ingredients of Portland clinker, which leads to formation and release of CO_2, and (ii) high energy consumption during its manufacturing, including heating raw materials within a rotating kiln [1]. Thus, the construction sector is very interested in the development of new cementitious binders as an alternative to OPC.

One of the most promising emerging solutions is based on the production of clinker free cements, based on wastes and industrial by-products, referred to as alkali-activated cements, which are produced via the chemical reaction of a poorly crystalline precursor with a highly alkaline solution, forming a hardened solid [2]. One of the most widely used precursors for production of alkali-activated cements is fly ash, derived from the combustion of coal in thermal stations [3]. Alkali-activated fly ash (AAFA), has been extensively studied over the past decades [4–7], and its mechanical and

durability performance is strongly dependent on the type of fly ash [8] and activating conditions used [9].

Several studies [10,11] have demonstrated carbon steel reinforcements are compatible with AAFA mortars, showing reduced corrosion rates than those recorded in OPC mortars. Reinforcing carbon steel embedded in carbonated AAFA mortars partially immersed in a water solution containing 1% (by binder weight) chlorides showed [10] linear polarization resistance (LPR) values one order of magnitude higher than those measured for OPC mortars. The resulting corrosion current density (i_{corr}) was about 0.9 and 0.2–0.5 μA cm^{-2} for OPC and AAFA mortars, respectively, indicating lower corrosion rates in alternative cementitious based solely on AAFA. Consistent results were identified in naturally carbonated AAFA concretes [12] where long-term electrochemical testing showed that the high alkalinity of these systems promoted the passivation of the steel rebar during the first 200 days after casting. In the case of alkali-activated concretes based on low-Ca fly ashes, the corrosion potential (E_{corr}) values were within the range of minimal corrosion risk, while the higher-Ca fly ash based concretes presented E_{corr} values within the range of high risk of corrosion of the steel rebars.

Corrosion of reinforced steel is one of the main causes of the premature failure of reinforced concrete structures (RCS). The passivity of reinforcing steel in concrete is frequently attributed to the formation on its surface of a thin passive film, whose growth and stability is dependent on the high pH of the surrounding concrete [13,14]. The onset of corrosion in RCS can be accelerated by the presence of chlorides ions or CO_2. When the chloride ions reach the metal/concrete interface produce pits on the surface of the steel, and localized corrosion takes place [15], while in the presence of CO_2 the passive

film may be destroyed when this reacts with the hydrated cement matrix and lowers the pH (under the value of 9), leading to generalized corrosion attack [16].

Corrosion protection of RCS is often achieved by adding corrosion inhibitors to the concrete, using high performance concrete mixtures, protective coatings or stainless steel rebars, or applying cathodic protection systems. Among these methods, the use of protective coatings is attractive from a protection point of view because of their low cost compared to other protection methods such as cathodic protection or the use of galvanized or stainless steel. Moreover, they can establish a physical barrier between aggressive ions and the steel rebars [17,18].

In the past years, the sol-gel process has proved to be a useful method for obtaining protective coatings to be applied on a wide variety of materials: glasses [19], ceramics [20], organic materials [21], metals like copper [22], aluminium and its alloys [23], stainless steel [24] and carbon steel [25]. The sol-gel process is a chemical route based on hydrolysis of various alkoxides to form respective silanols [26–29]. This is followed by a condensation reaction occurring between silanols or silanols and alkoxides. The sol-gel process involves evolution of inorganic networks through the formation of a colloidal suspension (sol) and gelation of the sol to form a network in a continuous liquid phase (gel). The precursors for syntheses of such colloids consist of metal or metalloid elements surrounded by various reactive ligands. Metal alkoxides are the often used because of their high reactivity with water. The most widely alkoxides utilized are alkoxysilanes such as tetraethyl orthosilicate (TEOS). In addition, it should be mention the existence of alkoxysilane precursors modified with a polymerizable *R* group, such as epoxy, methacrylic or acrylic organofunctional species. A common compound with polymerizable organic groups is 3-methacryloxy-propyltrimethoxysilane (MPTS). The main advantages of this process are: low cost of

production, high efficiency, good adherence to the substrate, low processing temperature, high homogeneity of the final product and resistance against corrosion and oxidation, homogeneity of the treated surfaces and high mechanical and chemical resistance.

Depending on the nature of the coatings, they can be inorganic (when they are prepared starting from metal alkoxides precursors) [30], and hybrid organic-inorganic (obtained including organic groups in the inorganic network in order to obtain thicker layers and/or flexible films) [31]. The organic-inorganic hybrid materials have attracted particular interest in the microelectronic and optic industries because of their excellent properties, such as molecular homogeneity, transparency, flexibility, rigidity, durability and excellent mechanical properties [28].

In recent studies by the authors [32,33], the thicknesses and compositions of four types of hybrid organic-inorganic coatings produced with tetraethyl orthosilicate (TEOS), 3-methacryloxy-propyl-trimethoxysilane (MPTS), methyl-triethoxysilane (MTES) and tetramethyl orthosilicate (TMOS) and varying molar ratios, have been produced, and its corrosion performance when deposited in steel rebars immersed in simulated concrete pore (SCP) solutions contaminated with chloride or in a carbonated synthetic solution simulating the carbonated concrete pore (SCCP) solution was assessed. The results showed that all the organic-inorganic coatings produced improve the corrosion resistance of carbon steel when exposed to both aggressive media; however their effectiveness is strongly dependent on the nature of the reagents used.

In the present study the protective properties of a hybrid organic-inorganic coatings prepared via sol-gel with a molar ratio of 1.0 deposited in carbon steels are assessed using electrochemical techniques including LPR and electrochemical impedance spectroscopy (EIS) method. The coated rebars were embedded in carbonated

OPC and AAFA mortars and immersed in a 3 wt. % sodium chloride (NaCl) solution up to 240 days.

2 EXPERIMENTAL METHODOLOGY

2.1 Preparation of Coated Steel Reinforcing Bars

Sol-gel coatings were prepared by condensation and polymerization of TEOS ($Si(OCH_2CH_3)_4$) and MPTS ($CH_2=C(CH_3)COO(CH_2)_3Si(OCH_3)_3$); TEOS and MTES ($(CH_3)Si(OCH_2CH_3)_3$); TMOS ($Si(OCH_3)_4$) and MPTS; or TMOS and MTES. All the reagents used were analytical grade from Sigma-Aldrich. As described in detail elsewhere [34], sol-gel coatings were prepared by mixing 5 g of MPTS or MTES with TEOS or TMOS using a molar ratio of 1.0. This molar ratio was selected based on the reported in [32–33], where it was determined that a molar ratio of 0.5 was insufficient to obtain a protective hybrid organic-inorganic film against the corrosion, and the use of a molar ratio of 2.0 may increase the price of the coatings synthesis, without much better protective properties when compared with coatings produced with a molar ratio of 1.0.

Carbon steel bars with 10 mm in diameter and 100 mm in height were used for electrochemical tests. Their chemical composition (% by weight) was 0.45 C, 0.22 Si, 0.72 Mn, <0.010 P, 0.022 S, 0.13 Cr, 0.13 Ni, 0.18 Cu, and balance Fe. The carbon steel bars were dipped in the hybrid organic-inorganic solutions, withdrawn at a rate of 14 mm min^{-1}, and air-dried for approximately 10 min. This procedure was carried out twice, after which the coated steels were heated at 65 ºC for 24 h and cured at 160 ºC for 3 h.

2.2 Preparation of Prismatic Mortars

A commercial Portland cement type I (42.5 R) and a Class F fly ash (FA), obtained from a steam power plant in Córdoba, Spain, were used as binding materials to

produce the mortar slabs. The chemical compositions and Blaine finesses of the materials (Spanish/European Standard UNE–EN 196–6) are shown in Table 1.

As alkaline activator a solution containing 85 wt.% of 10M NaOH and 15 wt.% of sodium silicate was used. The products used to prepare this solution were laboratory grade reagents, sodium hydroxide (NaOH) pellets (Panreac) and sodium silicate or waterglass containing 27% SiO_2, 8.2% NaOH and 64.8% H_2O (Merk). The sand:OPC and sand:FA ratio used in the mortars was 3.0. A standardized, evenly graded siliceous sand was employed (SiO_2 content of 99%, where 66% of particles with size <1 mm and 35% <0.5 mm). In all mortar types the liquid:binder ratio was 0.6 to favour carbonation process.

Prismatic mortar specimens, with dimensions 8 cm × 5.5 cm × 2 cm, similar to those used in a previous work [35] were prepared, each embedding two coated carbon steel bars ~~with polysiloxane hybrids synthesized from the TEOS/MPTS, TEOS/MTES, TMOS/MPTS or TMOS/MTES mixtures using a molar ratio of 1.0~~, as illustrated in Fig 1. Two specimens were prepared from each mortar/steel system, corresponding to four tested bars for each condition. OPC and AAFA mortars underwent hardening and carbonation steps, according to the conditions specified in Table 2 [36].

The completion of the carbonation reaction was checked on cubic samples (side 10 cm), produced and carbonated under similar conditions to those specified (Table 2) for the reinforced slabs. The cubes were sectioned at different times of CO_2 exposure, and the carbonation depths were monitored by spraying freshly cut surfaces with a 1% phenolphthalein solution. Thereafter, without any previous water pre-saturation, the samples were partially immersed (2.5 cm from the bottom of the sample) in a 3 wt.% NaCl solution for up to 240 days, at room temperature and open to the air.

2.3 Electrochemical Measurements

E_{corr}, LPR and EIS measurements were recorded after 1, 7, 30, 60, 90, 120 and 240 days of partial immersion of the specimens in a 3 wt.% NaCl solution. The NaCl solution was replaced by fresh solution after each measurement to avoid contamination of the electrolyte, and to maintain constant the concentration of chlorides in the solution.

For the electrochemical measurements a three-electrode configuration was used, consisting of an external stainless steel cylinder of 5 cm diameter carrying a centrally drilled hole as counter electrode, a saturated calomel electrode (SCE) positioned in the hole as reference electrode, and the coated steels embedded in the prismatic mortars as working electrode. A pad soaked in tap water was used to facilitate the electrical measurements. On the working electrode the exposed steel surface area was controlled covering it with adhesive tape, leaving an active surface area of 10 cm^2.

A PARC 273A Potentiostat and a Solartron 1250 FRA were utilized for the electrochemical measurements. LPR was obtained by applying a ΔE of ±15 mV vs. E_{corr}, at a scan rate of 0.1667 mV s^{-1}. The i_{corr} was calculated using the Stern-Geary equation [37]: $i_{corr} = B/R_p$, adopting a tentative B value of 52 mV or 26 mV for carbon steel in the passive or active (corroding) state, respectively [38]. EIS measurements were recorded at the E_{corr} in a frequency range from 64 kHz to 10 mHz with a logarithmic sweeping frequency of 5 points per decade. EIS involved the imposition of a 10 mV rms amplitude excitation voltage. Both LPR and EIS measurements were performed after the E_{corr} was stabilized for at least 30 min.

3 RESULTS AND DISCUSSION

3.1 Evolution of Corrosion Potential and Corrosion Current Density

Fig. 2 shows the variation in E_{corr} for carbonated OPC mortar samples with uncoated and coated steel rebars as function of the immersion time in the NaCl rich solution. The E_{corr} of uncoated rebar embedded in OPC mortar always showed very negative (between –570 and –640 mV vs. SCE) during all the exposure period. According to ASTM C876–09 standard [39], if the E_{corr} of a reinforcement embedded in concrete is more negative than –270 mV vs. SCE, there is a high risk of corrosion with 90% probability. The E_{corr} of coated rebars embedded in OPC mortars, as shown in Fig. 2, were between –560 mV vs. SCE and –690 mV vs. SCE, corresponding to an active state. These shifts of potential to more negative values also indicated that the mortar presented a low resistivity. The typical ranges of the potential of normal steel in low resistive concrete (wet and chloride contaminated) are between –400 mV vs. SCE and –600 mV vs. SCE according to RILEM TC 154-EMC Recommendations [40]. Similar values were obtained for the uncoated steel, during the first days of immersion. The initiation of corrosion of uncoated steel rebar embedded in mortar specimen is likely a consequence of the breakdown of the passive film induced by the chloride ions and/or the potential increase in the permeability of the samples, the samples presented a low resistivity (more open pore structure) and a transport of chlorides easier into concrete [40-42]. For specimens with coated steel rebar, the corrosion mechanism is likely controlled by the penetration of chloride through the existing defects in the coating initiating the corrosion process.

For the carbonated AAFA mortars immersed in the NaCl solution it was observed (Fig. 2) that the control rebar and coated steel with polysiloxane hybrids synthesized from the TEOS/MPTS mixture crossed the threshold potential limit of –270 mV vs. SCE within 7 days of exposure, indicating the possibility of corrosion

occurrence of more than 90%. The E_{corr} of the other coated steel rebars was –270 mV vs. SCE up to 30 days of immersion, and then shifted negatively to about –550 to –580 mV vs. SCE. These coated rebars remained in a passive state for more time (between 7 and 30 days instead of 1 and 7 days).

The measured values of i_{corr}, using the LPR method, for the uncoated and coated steel rebars embedded in carbonated systems at different time intervals of exposure are shown in Fig. 3. The criteria used for analysing these results are based on the state of corrosion of steel in concrete reported in [43-45], where a i_{corr} <0.1 µA cm^{-2} corresponds to passivity, a 0.1 µA cm^{-2} < i_{corr} < 0.5 µA cm^{-2} corresponds to low corrosion, for 0.5 µA cm^{-2} < i_{corr} < 1.0 µA cm^{-2} high corrosion, and for i_{corr} > 1.0 µA cm^{-2} very high corrosion. The i_{corr} of the control rebar embedded in OPC mortar specimens was 0.8 µA cm^{-2} after 7 days of immersion, the corrosion level was high and it increased rapidly to 1–10 µA cm^{-2}, with extended time of chlorides exposure, indicating a very high corrosion. The coated steel rebar with polysiloxane hybrids synthesized from the TEOS/MPTS mixture had the lowest i_{corr} at 7 days of exposure (see Fig. 3). However, a progressive increase of i_{corr} value was observed for this coated rebar and when using the other organic-inorganic films, as a consequence of their deterioration in the presence of chloride ions, indicating that their protective properties were not always good.

The i_{corr} values of uncoated and coated rebars embedded in carbonated AAFA mortar specimens immersed in 3 wt.% NaCl solution are also shown in Fig. 3. During the first days of immersion (~1 week), all steel rebars exhibited i_{corr} values of the order of 0.05 µA cm^{-2}, except for the uncoated steel and the coated steel rebars with organic-inorganic hybrids synthesized from the TMOS/MPTS mixture, whose i_{corr} values were

higher, 0.18 μA cm^{-2} and 0.29 μA cm^{-2}, respectively. After 60 days of immersion, the corrosion level for the uncoated steel and the coated steel rebars with organic-inorganic hybrids synthesized from the TMOS/MPTS and TEOS/MPTS mixtures was high (0.5 μA cm^{-2} < i_{corr} < 1 μA cm^{-2}), while than that of the others coated rebars which was low (0.1 μA cm^{-2} < i_{corr} < 1 μA cm^{-2}) [43-45]. After 90 days of immersion, all the samples showed similar i_{corr} values of around 1.9 μA cm^{-2}. These values were maintained roughly constant throughout the immersion time, except for the coated steel rebar with organic-inorganic hybrids synthesized from the TEOS/MTES mixture that exhibited the lowest i_{corr} value. This coated steel rebar embedded in carbonated AAFA mortar exhibited the best protective properties during 240 days of immersion.

The decrease in the E_{corr} values and the increase in i_{corr} values upon the time of immersion in the chlorides rich solution indicate the gradual penetration of electrolyte through the defects and the irregularities in the coatings. This result suggests that even in the presence of the different coatings, active corrosion occurs under the coating layer after a particular immersion time, consistent with the reported by Pour-Ali et al. [17].

The higher E_{corr} values and the lower i_{corr} values of TEOS/MTES and TMOS/MTES coated steel rebars embedded in carbonated AAFA mortars may be attributed to the establishment of a physical barrier against aggressive ions by deposition of these more protective coatings on the metal surface.

In light of the results, the type of the cementitious matrix (Portland or fly ash) had a notable influence in the onset of corrosion of coated steel rebars. This is expected as both systems present wide differences in the chemical compositions of their main reaction products: calcium silicate hydrated (C–S–H) gel of the hydration of Portland cement [46] and alkaline aluminosilicate hydrated (N–A–S–H) gel generated as a result

of fly ash activation [47]; in the reaction mechanisms involved in the production of the two types of gel and in the kinetic of the formation processes. It is also important to stress that the exact chemical composition of the pore solution of the cementitious matrix is quite complex to determine, and varies with the type of cement, water:cement ratio, degree of hydration and exposure conditions, and therefore the presence of determined species in the pore solution could influence on corrosion process.

Moreover, porosity is known to affect not only mechanical strength but durability as well, for high porosity further the ingress of aggressive agents such as chloride ions into the material. A. Fernandez-Jimenez et al. [48] determined the effective porosity and pore size distribution for Portland cement and activated fly ash mortar. These samples were similar to those used in this research, but with different liquid/binder ratio. OPC and fly ash activated with sodium silicate and sodium hydroxide solution had porosity values of 7.6 and 9.6%, respectively. These values were very close and both materials could present similar corrosion performance. In other study carried out by the authors [11] also indicate the presence of a comparable permeability in OPC and fly ash alkali activated mortars, with the same ratio liquid/binder used in this study. The results showed that at the end of exposure period the carbonated mortars presented a pH value of about 9.5 and the concentrations of soluble chlorides (in wt% vs binder) were: 0.44 ± 0.11 in OPC and 0.37 ± 0.06 in fly ash activated with sodium silicate and sodium hydroxide solution mortars.

It should be also considered that the fly ash was activated with a blend of NaOH and sodium silicate, and therefore the electrolyte present in these mortar pores could act as a corrosion inhibitor hindering steel corrosion. Silicate anions are known to be corrosion inhibitors for iron and steel [49,50]. These authors observed that the Fe(II) dissolution current values were smaller in the solution containing silicate, which may be explained by assuming that the passive film ionic resistivity is bigger when silicate was

present in solution. This behaviour was probably due to its incorporation into the film, which reduces the ferrous species dissolution. Therefore, the significant concentration of silicate in the electrolyte of AAFA mortars may be the cause of the better corrosion behaviour of steel in these mortars than in OPC mortars.

On the other hand, the TEOS or TMOS/MTES formulations had a denser and more compact structure, the degree of the condensation was between 82–85% and the *d* parameter was between 2.86–2.99 [34]. In addition, these coatings presented a large number of covalent bonds, higher atomic percentage of Si in their compositions [33], and strong adhesion between the coating and the steel substrate, and thus less susceptible to debonding and delamination of the coatings. Therefore, these polysiloxane hybrid films provided a more effective physical barrier preventing the penetration of the electrolyte, promoting a lower corrosion tendency in carbonated AAFA mortars up to 60 days of exposure to a rich chlorides solution.

3.2 EIS Results

Fig. 4 shows the Nyquist plots for uncoated steel rebar in carbonated OPC and AAFA mortars during 240 days of immersion in 3 wt.% NaCl solution. They showed three time constants regardless of immersion time. At frequencies higher than 10^3 Hz the spectra showed a semicircle characterising the dielectric properties of the bulk matrix [51]. In some cases, only a section of this semicircle was observed within the available instrumental frequency range. The second time constant in the intermediate frequency range (usually in the 10^3–1 Hz range for OPC mortars and in the 10^3–10 Hz range for AAFA mortars) was attributed to the properties of the passive layer formed on the steel rebar due to the high pH of OPC or AAFA pore solutions. The third time constant in the low frequency range (<1 or 10 Hz for OPC and AAFA mortars, respectively) was related to the interface properties between steel rebar and mortar

where corrosion occurred, namely the charge transfer resistance (R_{ct}) and double-layer capacitance (Y_{dl}).

Fig. 5 depicts the Nyquist plots for coated rebars embedded in carbonated OPC and AAFA mortars during 240 days of immersion in 3 wt.% NaCl solution. These specimens also presented three time constants, which appeared in the same range of frequencies that those observed for uncoated rebars in both mortars (Fig. 4), except for the first time constant of OPC mortars that appeared at frequencies higher than 10^2 Hz. However, in these cases, the first time constant was also attributed to the dielectric properties of the bulk matrix, the second time constant was associated with the presence of the hybrid coating layer and finally, the third time constant was also related to the corrosion process occurring at the steel/mortar interface.

These three time constants were more difficult to detect in the fly ash system, since all three capacities were between 10^{-5} and 10^{-4} F cm^{-2} $s^{-(1-\alpha)}$, and were overlapping, but they were needed to explain the dielectric properties the bulk matrix, passive film or hybrid coatings and the interface properties between steel rebar and mortar or coating. By contrast, in the case of Portland cement system, the capacitance corresponding to high frequencies appeared between 10^{-8} and 10^{-7} F cm^{-2} $s^{-(1-\alpha)}$, the capacitance at medium frequency around of 10^{-5} and 10^{-4} F cm^{-2} $s^{-(1-\alpha)}$ and the capacitance at low frequency in the order of mF cm^{-2} $s^{-(1-\alpha)}$ and they were easily observable in the Nyquist diagram, see Figs. 4 and 5.

The dielectric properties of the bulk matrix, passive film or hybrid coating film as well as the electrochemical behaviour at the steel/mortar interface can be quantified by fitting an appropriate equivalent electrical circuit (EEC) model to the EIS data. In the present study, the EEC shown in Fig. 6 was utilized, using the *ZView* Software for the

fitting process. The chi-square (χ^2) value in all the cases was of the order of 10^{-3}, indicating a good fit. In the EEC a constant phase element (*CPE*) was used instead of a pure capacitor in order to consider the non-homogeneity of the system studied, which mainly comes from the irregularities on the steel surface, surface roughness, fractal surface and in general certain processes associated with an irregular distribution of the applied potential [11,41]. The electrical impedance of a *CPE* is defined by the expression:

$$Z_{CPE} = \left(Y_p\right)^{-1}\left(j\omega\right)^{-\alpha} \quad (1)$$

where Y_p is the admittance, ω is the angular frequency equal to $2\pi f$, f is the applied frequency, 2π is the habitual conversion constant, $j^2=(-1)$ is the imaginary unit, and α, defined as the *CPE* power, is in the range $-1 < \alpha < 1$. When $\alpha=0$, *CPE* is a resistor; when $\alpha=1$, it is an ideal capacitor; and when $\alpha=-1$, it is an inductor. Finally, if $\alpha=0.5$, the *CPE* is the Warburg admittance. R_e in Fig. 6 accounts for the electrolyte resistance. The electrolyte resistance is associated with the ionic mobility in a solution. R_m and Y_m are associated with the bulk matrix resistance and capacitance, respectively. The bulk matrix resistance reflects the ability of the mortar to resist the penetration of electrolytes containing aggressive ions and the bulk matrix capacitance reflects the dielectric properties of the mortars. R_f and Y_f indicate the passive film or hybrid coating film resistance and capacitance, respectively. Finally, R_{ct} and Y_{dl} are associated with the charge transfer resistance of the corrosion process and the double-layer capacitance, respectively. A model similar to this was used to study the electrochemical characteristics of enamel coated steel rebar embedded in OPC mortars [41].

Tables 3 and 4 list EEC parameter values obtained by fitting the Nyquist plots recorded for carbonated OPC and AAFA mortars with the uncoated steel rebar after

different times (up to 240 days) of immersion in the NaCl rich solution. R_e values showed a tendency to increase over exposure time in OPC mortars, probably due to the mortar curing process, which induced a long-term decrease in the mortar porosity and an increase in its resistivity. R_e values were in the range from 110 and 347 Ω cm^2 for AAFA mortars. This decrease in the R_e parameter may be attributed to a high concentration of dissolved salts in the mortar pore network solution.

R_m parameter was in the range of 416–1863 Ω cm^2 for uncoated steel embedded in carbonated OPC mortars, and in the range of 28–163 Ω cm^2 for uncoated steel embedded in carbonated AAFA mortars. Y_m parameter was in the range of 61–1061 nF cm^{-2} $s^{-(1-\alpha_{HF})}$ for OPC mortars and 1–36 µF cm^{-2} $s^{-(1-\alpha_{HF})}$ for AAFA mortars. These lower R_m values and higher Y_m values for AAFA mortars may be due the formation of different reaction products in the cementitious systems, and the presence of a more electrically conductive solution inside the carbonated AAFA mortars, than those in OPC mortars. In AAFA mortars the penetration of CO_2 favoured the formation of sodium carbonate while in the OPC mortars produced the more insoluble calcium carbonate [10,52].

At intermediate frequency, R_f parameter was in the range of 318–1269 Ω cm^2 and Y_f parameter was in the range of 67–480 µF cm^{-2} $s^{-(1-\alpha_{IF})}$ for the uncoated steel embedded in carbonated OPC mortars. For uncoated steel rebar embedded in carbonated AAFA mortars, R_f and Y_f values were of the same order of magnitude. Finally, at low frequencies R_{ct} parameter was as high as 3.3×10^6 Ω cm^2 for the uncoated steel embedded in AAFA mortars, and this parameter always was higher than for uncoated steel embedded in OPC mortars. This indicates a higher corrosion resistance of the steel reinforcement in these new mortar types (AAFA). R_{ct} displayed a continuous reduction

with time of immersion (~2–5 kΩ cm^2), indicating a transition from the passive state to the activate state. With the time, an increase of the concentration of chloride ions took place on the metal surface, more corrosion pits were formed on the passive film and its breakdown occurred. Y_{dl} parameter was in the range of 2–5 mF cm^{-2} $s^{-(1-\alpha_{LF})}$ for OPC mortars and in the range of 63–633 µF cm^{-2} $s^{-(1-\alpha_{LF})}$ for AAFA mortars. Y_{dl} values increased with exposure time for AAFA mortars, but these values were always lower than those for OPC mortars. The smallest Y_{dl} values of AAFA mortars also indicates a higher corrosion resistance.

Accepting that the Stern-Geary equation can be applied, with an approximate B constant value of 52 mV or 26 mV, the resulting i_{corr} was 1.04 µA/cm^2 for OPC mortar and 0.06 µA/cm^2 for AAFA mortar at 30 days, steels were in active and passive state respectively. These results were not far from the i_{corr} results obtained using lineal polarisation resistance measurements (see Fig. 3).

Tables 5 and 6 list EEC parameter values obtained by fitting the Nyquist plots recorded for carbonated OPC and AAFA mortars with the different coated steel rebars after different times (up to 240 days) of immersion in the NaCl rich solution. The R_e values for coated steels embedded in OPC mortars were in the range from 228 Ω cm^2 to 5469 Ω cm^2, while they were lower, between 46 and 319 Ω cm^2 in the case of coated steels embedded in AAFA mortars. This decrease in the R_e parameter may be which may be associated with a high level of sodium salts in the pores of the latter mortar when carbonated, which are present in the activating solutions [10,11].

Fig. 7 displays the changes in the bulk-matrix resistance (R_m) and capacitance (Y_m) parameters over the time for coated steel rebars synthesized with the TEOS/MPTS, TEOS/MTES, TMOS/MPTS or TMOS/MTES mixtures, and embedded in carbonated

OPC and AAFA mortars immersion in the NaCl rich solution. For OPC mortars R_m values were in the range of 208–6030 Ω cm^2, while for AAFA mortars were in the range of 3–192 Ω cm^2, which were approximately thirty times lower. OPC mortars had a higher resistivity than AAFA mortars, the open pore structure of OPC mortars was lower due to the calcium carbonate formed in these system was more insoluble thant sodium carbonate formed in AAFA system. Y_m values were in the ranges of 5–2970 nF cm^{-2} $s^{-(1-\alpha_{HF})}$ and 0.1–328 µF cm^{-2} $s^{-(1-\alpha_{HF})}$ for OPC and AAFA mortars, respectively. In most of the mortars assessed, these ranges were of the same order than obtained for the uncoated steel embedded in OPC and AAFA mortars. Moreover, the range of Y_m value for OPC mortars was in reasonable agreement with what has been reported in the literature [51,53].

Fig. 8 shows the changes in the R_f and Y_f parameters with time for coated steel with TEOS/MPTS, TEOS/MTES, TMOS/MPTS or TMOS/MTES mixtures embedded in carbonated OPC and AAFA mortars after different times of exposure to 3 wt.% NaCl solution. R_f and Y_f parameters measured the barrier performance of the hybrid coatings against the penetration of water and chloride ions [54,55]. R_f values for OPC mortars, independently of the coating deposited on the steel surface, were higher than those for AAFA mortars. This may be attributed to a slightly lower deterioration of the coating in this system, and a slower access of aggressive species to the steel. Y_f parameter varied in the range of 40–514 µF cm^{-2} $s^{-(1-\alpha_{IF})}$ for carbonated OPC mortars and of 61–540 µF cm^{-2} $s^{-(1-\alpha_{IF})}$ for carbonated AAFA mortars. The values of these latter mortars were higher than those for OPC mortars, indicating that the coatings deposited on the steel presented a slightly higher number of open channels allowing an easier water uptake.

Fig. 9 displays the changes in the R_{ct} and Y_{dl} parameters with time of the coated steel with TEOS/MPTS, TEOS/MTES, TMOS/MPTS or TMOS/MTES mixtures and embedded in carbonated OPC and AAFA mortars after different times of immersion in 3 wt.% NaCl solution. These parameters are associated with the corrosion process. For carbonated OPC mortars, R_{ct} values remained fairly constant over the time of immersion, within the range of 2.5×10^{3}–50.3×10^{3} kΩ cm^{2}. However, for carbonated AAFA mortars this parameter suffered a continuous reduction over the time of exposure to chlorides, presenting values within the range of 20.9×10^{6}–61.7×10^{3} Ω cm^{2}. After 240 days of exposure the R_{ct} values indicated that steel embedded in OPC mortar was in an active state, but the steels embedded in AAFA mortars remained in a passive state for longer period of time. The Y_{dl} parameter was in the range of 0.3–3.7 mF cm^{-2} $s^{-(1-\alpha_{LH})}$ for coated steel embedded in carbonated OPC mortars and of 75–6300 μF cm^{-2} $s^{-(1-\alpha_{LF})}$) for AAFA mortars. The smaller values of Y_{dl} indicate a higher corrosion resistance for this new type of mortar (AAFA), although these values at the end of the test were similar to those obtained for OPC mortars. This behaviour may indicate the increase of the activity of corrosion at the double-layer interface by the diffusion of chloride ions. In the light of the EIS results, carbonated AAFA mortars in the presence of chloride ions showed a higher corrosion resistance than OPC mortars likely due to the higher concentration of silicate anions in the pore solution of the AAFA mortars, capable of delaying the corrosion process [49,50]. A dense and compact structure, higher dimensionality and degree of condensation [34], and a greater adherence to the steel, higher atomic percentage of Si in their composition [33], lead to a low electrolyte diffusion rate through the film and protecting the steel rebar against corrosion. These

results are in agreement with those obtained using direct current (DC) measurements, shown in Fig. 3.

5 CONCLUSIONS

Corrosion of coated steel rebar embedded in carbonated OPC and AAFA mortars in the presence of chloride ions was not only dependent on the type of the cementitious system but also on the nature of reagents forming the coating. AAFA mortars were more efficient against rebar corrosion than OPC mortars (high E_{corr} values and low i_{corr} values), where the silicate present in the alkaline solution used for the activation of fly ash may act as a corrosion inhibitor of steel. The organic-inorganic hybrids synthesized with TEOS/MTES and TMOS/MTES for carbon steel embedded in carbonated AAFA mortars showed the lowest i_{corr} values, indicating that these coatings showed the best protective properties during 240 days of exposure.

Acknowledgements

M. Criado expresses her gratitude to the Spanish Ministry of Science and Innovation for the Juan de la Cierva contract (Ref. JDC–2010). Comments from Dr. S.A. Bernal (U. Sheffield) are greatly acknowledged.

REFERENCES

[1] E. Gartner, Industrially interesting approaches to "low-CO_2" cements, Cement Concrete Res. 34 (2004) 1489–1498.

[2] A. Palomo, P. Krivenko, I. Garcia-Lodeiro, E. Kavalerova, O. Maltseva, A. Fernández-Jiménez, A review on alkaline activation: new analytical perspectives, Mater. Constr. 64 (2014) e022.

[3] P. Duxson, J.L. Provis, Designing precursors for geopolymer cements, J. Am. Ceram. Soc. 91 (2008) 3864–3869.

[4] J. Davidovits, Geopolymers: Inorganic polymeric new materials, J. Therm. Anal. 37 (1991) 1633–1656.

[5] P. Duxson, A. Fernández-Jiménez, J.L. Provis, G.C. Lukey, A. Palomo, J.S.J. Van Deventer, Geopolymer technology: the current state of the art, J. Mater. Sci. 42 (2007) 2917–2933.

[6] A. Palomo, M.W. Grutzeck, M.T. Blanco, Alkali-activated fly ashes: A cement for the future, Cement Concrete Res. 29 (1999) 1323–1329.

[7] D. Hardjito, S.E. Wallah, D.M.J. Sumajouw, B.V. Rangan, On the development of fly ash-based geopolymer concrete, ACI Mater. J. 101 (2004) 467–472.

[8] F. Winnefeld, A. Leemann, M. Lucuk, P. Svoboda, M. Neuroth, Assessment of phase formation in alkali activated low and high calcium fly ashes in building materials, Constr. Build. Mater. 24 (2010) 1086–1093.

[9] A. Fernández-Jiménez, A. Palomo, Composition and microstructure of alkali activated fly ash binder: Effect of the activator, Cement Concrete Res. 35 (2005) 1984–1992.

[10] M. Criado, C. Monticelli, S. Fajardo, D. Gelli, V. Grassi, J.M. Bastidas, Organic corrosion inhibitor mixtures for reinforcing steel embedded in carbonated alkali-activated fly ash mortar, Constr. Build. Mater. 35 (2012) 30–37.

[11] C. Monticelli, M. Criado, S. Fajardo, J.M. Bastidas, M. Abbottoni, A. Balbo, Corrosion behaviour of a low Ni austenitic stainless steel in carbonated chloride-polluted alkali-activated fly ash mortar, Cement Concrete Res. 55 (2014) 49–58.

[12] M. Sufian Badar, K. Kupwade-Patil, S.A. Bernal, J.L. Provis, E.N. Allouche, Corrosion of steel bars induced by accelerated carbonation in low and high calcium fly ash geopolymer concretes, Constr. Build. Mater. 61 (2014) 79–89.

[13] L. Bertolini, B. Elsener, P. Pedeferri, R. Polder in: Corrosion of Steel in Concrete- Prevention, Diagnosis, Repair, Wiley-VCH, Weinheim, (2004).

[14] J.A. Gónzalez, Prediction of reinforced concrete structure durability by electrochemical techniques, Corrosion 63 (2007) 811–818.

[15] U. Angst, B. Elsener, C.K. Larsen, Ø. Vennesland, Critical chloride content in reinforced concrete-A review, Cement Concrete Res. 39 (2009) 1122–1138.

[16] N.M. Ihekwaba, B.B. Hope, C.M. Hansson, Carbonation and electrochemical chloride extraction from concrete, Cement Concrete Res. 26 (1996) 1095–1107.

[17] S. Pour-Ali, C, Dehghanian, A. Kosari, Corrosion protection of the reinforcing steels in chloride-laden concrete environment through epoxy/polyaniline–camphorsulfonate nanocomposite coating, Corros. Sci. 90 (2015) 239-247.

[18] M. Książek, The evaluate tendencies of corrosion process for reinforcing steel when covered with special polymer sulfur coating, Eng. Fail. Anal. 39 (2014) 1-11

[19] M. Barletta, M. Puopolo, A. Gisario, S. Vesco, Application and drying at ambient temperature of thick organic-inorganic hybrid coatings on glass, Surf. Coat. Tech. 236 (2013) 212-223.

[20] J.X Bi, C.H. Yang, H.T. Wu, Synthesis, characterization, and microwave dielectric properties of Ni0.5Ti0.5NbO4 ceramics through the aqueous sol-gel process, J. Alloy. Compd. 653 (2015) 1-6.

[21] J. Graffion, A.M. Cojocariu, X. Cattoën, R.A.S Ferreira, V.R. Fernandes, P.S. André, L.D. Carlos, M. Wong Chi Man, J.R. Bartlett, Luminescent coatings from bipyridine-based bridged silsesquioxanes containing Eu^{3+} and Tb^{3+} salts, J. Mater. Chem. 22 (2012) 13279-13285.

[22] E. Kiele, J. Senvaitiene, A. Griguceviciene, R. Ramanauskas, R. Raudonis, A. Kareiva, Application of sol-gel method for the conservation of copper alloys. Microchem. J. 124 (2016) 623-628.

[23] Z.N. Kayani, A. Munir, S. Riaz, S. Naseem, Structural, optical and magnetic properties of aluminum doped MnZnO films deposited by dip coating, J. Alloy. Compd. 662 (2016) 489-496.

[24] L. Ćurković, H.O. Ćurković, S. Salopek, M.M. Renjo, S. Šegota, Enhancement of corrosion protection of AISI 304 stainless steel by nanostructured sol-gel TiO_2 films, Corros. Sci. 77 (2013) 176-184.

[25] T.T. Phan, F. Bentiss, C. Jama, Structural and anticorrosion performance characterization of phosphosilicate sol-gel coatings prepared from 3-(trimethoxysilyl) propyl methacrylate and bis[2-(methacryloyloxy)ethyl] phosphate, Prog. Org. Coat. 89 (2015) 123-131.

[26] C.J. Brinker, G.W. Scherer, Sol-gel science, the physics and chemistry of sol-gel processing, Academic Press, San Diego, (1990).

[27] P. Judeinstein, C.J. Sanchez, Hybrid organic-inorganic materials: a land of multidisciplinarity, J. Mater. Chem. 6 (1996) 511–525.

[28] I. Zaręba-Grodź, W. Miśta, W. Stręk, E. Bukowska, K. Hermanowicz, K. Maruszewski, Synthesis and properties of an inorganic-organic hybrid prepared by the sol-gel method, Opt. Mater. 26 (2004) 207–211.

[29] M. Houmard, D.C.L. Vasconcelos, W.L. Vasconcelos, G. Berthomé, J.C. Joud, M. Langlet, Water and oil wettability of hybrid organic-inorganic titanate-silicate thin films deposited via a sol-gel route, Surf. Sci. 603 (2009) 2698–2707.

[30] T. Minami, N. Tohge, Formation of inorganic coatings on polymer films by the sol-gel method, New Glass 9 (1994) 23–28.

[31] V. Barranco, N. Carmona, J.C. Galván, M. Grobelny, L. Kwiatkowski, M.A. Villegas, Electrochemical study of tailored sol-gel thin films as pre-treatment prior to organic coating for AZ91 magnesium alloy, Prog. Org. Coat. 68 (2010) 347–355.

[32] M. Criado, I. Sobrados, J. Sanz, J.M. Bastidas, Steel protection using sol-gel coatings in simulated concrete pore solution contaminated with chlorides, Surf. Coat. Technol. 258 (2014) 485–494.

[33] M. Criado, I. Sobrados, J.M. Bastidas, J. Sanz, Steel corrosion in simulated carbonated concrete pore solution its protection using sol-gel coatings, Prog. Org. Coat. 88 (2015) 228–236.

[34] M. Criado, I. Sobrados, J. Sanz, Polymerization of hybrid organic-inorganic materials from several silicon compounds followed by TGA/DTA, FTIR and NMR techniques, Prog. Org. Coat. 77 (2014) 880–891.

[35] M. Criado, I. García-Díaz, J.M. Bastidas, F.J. Alguacil, F.A. López, C. Monticelli, Effect of recycled glass fiber on the corrosion behavior of reinforced mortar, Constr. Build. Mater. 64 (2014) 261–269.

[36] ASTM E104–02 Standard, "Maintaining Constant Relative Humidity by Means of Aqueous Solutions".

[37] M. Stern, A.L. Geary, Electrochemical polarization I. A theoretical analysis of the shape of polarization curves, J. Electrochem. Soc. 104 (1957) 56–63.

[38] C. Andrade, V. Castelo, C. Alonso, J.A. González, The determination of the corrosion rate of steel embedded in concrete by the polarization resistance and AC impedance methods. In: STP 906, Corrosion of Rebar in Concrete, ASTM, Philadelphia, PA, (1984).

[39] ASTM C876–09 Standard, “Test Method for Half-Cell Potentials of Uncoated Reinforcing Steel in Concrete”.

[40] B. Elsener, C. Andrade, J. Gulikers, R. Polder, M. Raupach, RILEM TC 154-EMC Recommendations: Half-cell potential measurements-Potential mapping on reinforced concrete structueres, Mater. Struct. 36 (2003) 461-471.

[41] F. Tang, G. Chen, J.S. Volz, R.K. Brow, M.L. Koenigstein, Cement-modified enamel coating for enhanced corrosion resistance of steel reinforcing bars, Cement Concrete Comp. 35 (2013) 171–180.

[42] T. Zafeiropoulou, E. Rakanta, G. Batis, Performance evaluation of organic coatings against corrosion in reinforced cement mortars, Prog. Org. Coat. 72 (2011) 175–180.

[43] Durar network specification manual inspection evaluation and assessment of Corrosion in reinforced concrete structures, CYTED Program, Rio de Janeiro, (1997).

[44] G. Fajardo, P. Valdez, J. Pacheco, Corrosion of steel rebar embedded in natural pozzolan based mortars exposed to chlorides, Construc. Build. Mater. 23 (2009) 768-774.

[45] P. Garcés, L.G. Andión, E. Zornoza, M. Bonilla, J. Payá, The effect of processed fly ashes on the durability and the corrosion of steel rebars embedded in cement–modified fly ash mortars, Cement Concrete Compos. 32 (2010) 204-210.

[46] H.F.W. Taylor, Cement Chemistry, Academic Press, London, (1990).

[47] A. Palomo, S. Alonso, A. Fernández-Jiménez, I. Sobrados, J. Sanz, Alkaline activation of fly ashes. A ^{29}Si NMR study of the reactions products, J. Am. Ceram. Soc. 87 (2004) 1141–1145.

[48] A. Fernandez-Jimenez, J.M. Miranda, J.A. Gonzalez, A. Palomo, Steel passive state stability in activated fly ash mortars, Mater. Construc. 60 (2010) 51-65.

[49] S.T. Amaral, I.I. Müller, Passivation of pure iron in alkaline solution containing silicate and sulphate-galvanostatic and potentiostatic studies, Corros. Sci. 41 (1999) 747–758.

[50] S.T. Amaral, I.I. Müller, A RRDE study of the electrochemical behavior of iron in solutions containing silicate and sulphate at pH 10–13, Corros. Sci. 41 (1999) 759–771.

[51] K.K. Sagoe-Crentsil, F.P. Glasser, J.T.S. Irvine, Electrochemical characteristics of reinforced concrete corrosion as determined by impedance spectroscopy. Brit. Corros. J. 27 (1992) 113–118.

[52] S.A. Bernal, J.L. Provis, B. Walkley, R. San Nicolas, J.D. Gehman, D.G. Brice, A.R. Kilcullen, P. Duxson, J.S.J. van Deventer, Gel nanostructure in alkali-activated binders based on slag and fly ash, and effects of accelerated carbonation. Cement Concrete Res. 53 (2013) 127–144.

[53] W. Aperador, R. Mejía de Gutiérrez, D.M. Bastidas, Steel corrosion behaviour in carbonated alkali-activated slag concrete, Corros. Sci. 51 (2009) 2027–2033.

[54] F. Tang, G. Chen, R.K. Brow, J.S. Volz, M.L. Koenigstein, Corrosion resistance and mechanism of steel rebar coated with three types of enamel, Corros. Sci. 59 (2012) 157–168.

[55] F. Tang, X. Chen, G. Chen, R.K. Brow, J.S. Volz, M.L. Koenigstein, Electrochemical behavior of enamel-coated carbon steel in simulated concrete pore water solution with various chloride concentrations, Electrochim. Acta 92 (2013) 36–46.

FIGURE CAPTIONS

Fig. 1. Photography of a prismatic mortar specimen studied.

Fig. 2. Corrosion potential (E_{corr}) evolution of the uncoated and coated steel rebars embedded in carbonated OPC and AAFA mortars, over the time of immersion in a 3 wt.% NaCl solution.

Fig. 3. Corrosion current density (i_{corr}) evolution of uncoated and coated steel rebars embedded in carbonated OPC and AAFA mortars, over the time of immersion in a 3 wt.% NaCl solution.

Fig. 4. Nyquist plots of the carbonated OPC and AAFA mortars reinforced with uncoated steel rebar during 240 days of immersion in a 3 wt.% NaCl solution.

Fig. 5. Nyquist plots for coated rebars embedded in carbonated OPC and AAFA mortars during 240 days of immersion in a 3 wt.% NaCl solution.

Fig. 6. Equivalent electrical circuit (EEC) for carbonated OPC and AAFA with uncoated and coated steel rebar.

Fig. 7. Bulk-matrix resistance (R_m) and capacitance (Y_m) values of the coated steel rebars synthesized with the TEOS/MPTS, TEOS/MTES, TMOS/MPTS or TMOS/MTES mixtures and embedded in carbonated OPC and AAFA mortars during 240 days of immersion in a 3 wt.% NaCl solution. Left: R_m. Right: Y_m.

Fig. 8. Coating resistance (R_f) and capacitance (Y_f) values of the coated steel rebars synthesized with the TEOS/MPTS, TEOS/MTES, TMOS/MPTS or TMOS/MTES mixtures and embedded in carbonated OPC and AAFA mortars during 240 days of immersion in a 3 wt.% NaCl solution. Left: R_f. Right: Y_f.

Fig. 9. Charge transfer resistance (R_{ct}) and double-layer capacitance (Y_{dl}) values of the coated steel rebars synthesized with the TEOS/MPTS, TEOS/MTES, TMOS/MPTS or TMOS/MTES mixtures and embedded in carbonated OPC and AAFA mortars during

240 days of immersion in a 3 wt.% NaCl solution. Left: R_{ct}. Right: Y_{dl}.

Fig. 1

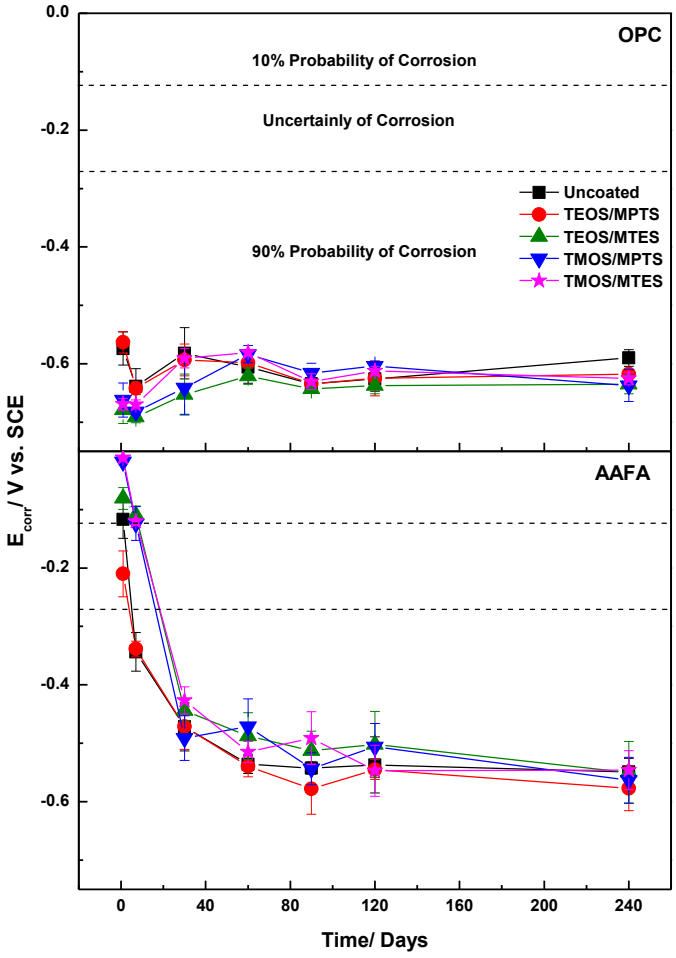
OPC
10% Probability of Corrosion
Uncertainly of Corrosion
90% Probability of Corrosion
Uncoated
TEOS/MPTS
TEOS/MTES
TMOS/MPTS
TMOS/MTES
AAFA
E_{corr} / V vs. SCE
Time/ Days
0.0
-0.2
-0.4
-0.6
0
40
80
120
160
200
240

Fig. 2

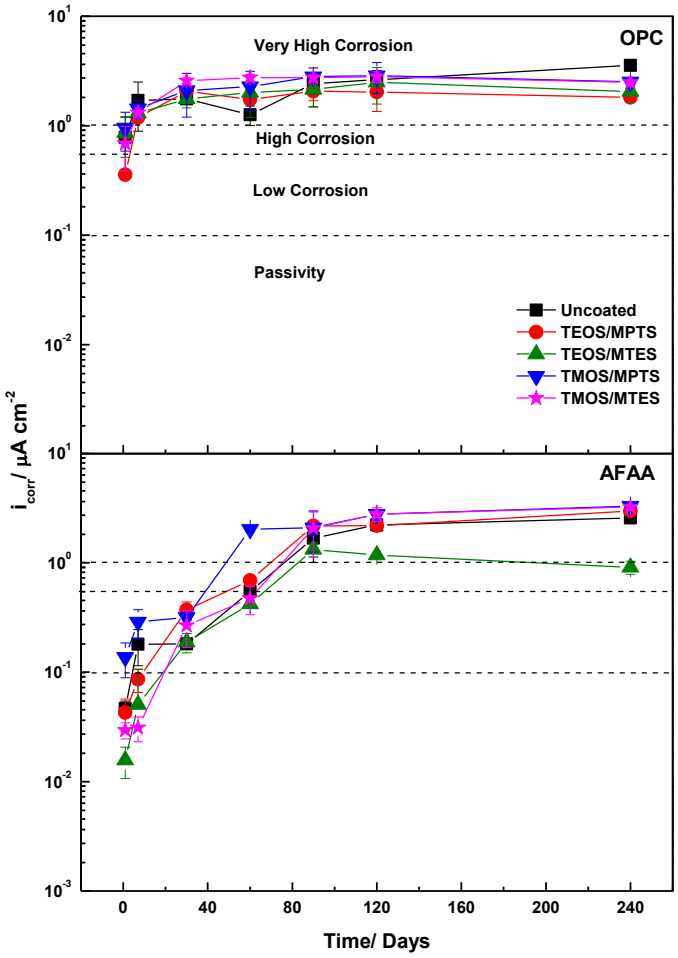
OPC
Very High Corrosion
High Corrosion
Low Corrosion
Passivity
Uncoated
TEOS/MPTS
TEOS/MTES
TMOS/MPTS
TMOS/MTES
AFAA
i_{corr} / µA cm^{-2}
Time/ Days

Fig. 3

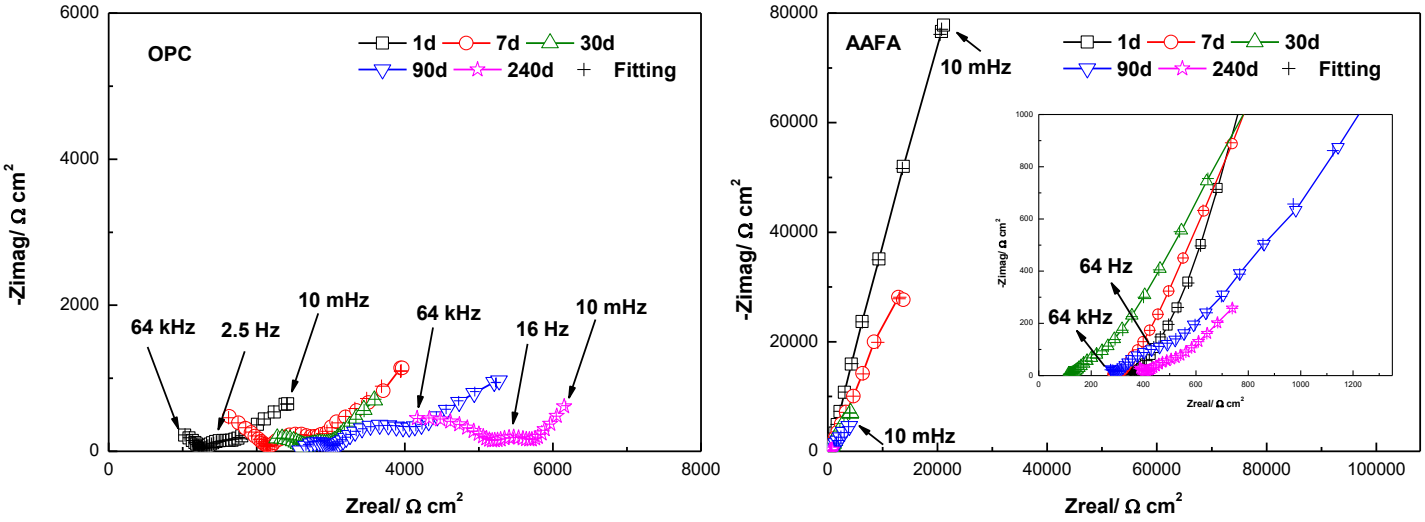
OPC
1d
7d
30d
90d
240d
Fitting
64 kHz
2.5 Hz
10 mHz
64 kHz
16 Hz
10 mHz
-Zimag/ Ω cm2
Zreal/ Ω cm2
AAFA
10 mHz
64 Hz
64 kHz
10 mHz

Fig. 4

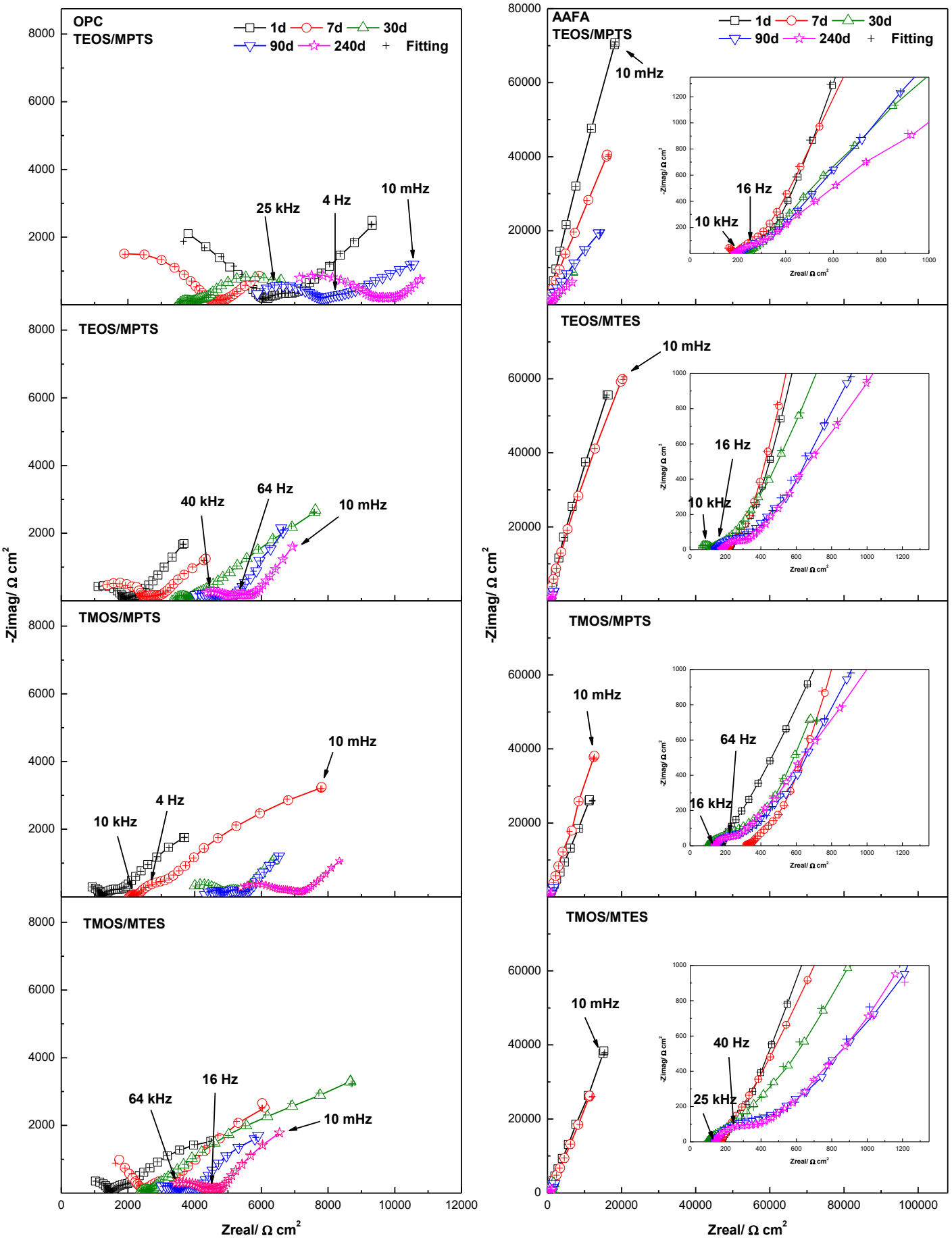
OPC
TEOS/MPTS
1d 7d 30d
90d 240d + Fitting
25 kHz
4 Hz
10 mHz
TEOS/MPTS
40 kHz
64 Hz
10 mHz
TMOS/MPTS
10 mHz
4 Hz
10 kHz
TMOS/MTES
64 kHz
16 Hz
10 mHz
AAFA
TEOS/MPTS
1d 7d 30d
90d 240d + Fitting
10 mHz
16 Hz
10 kHz
TEOS/MTES
10 mHz
16 Hz
10 kHz
TMOS/MPTS
10 mHz
64 Hz
16 kHz
TMOS/MTES
10 mHz
40 Hz
25 kHz
-Zimag/ Ω cm2
Zreal/ Ω cm2

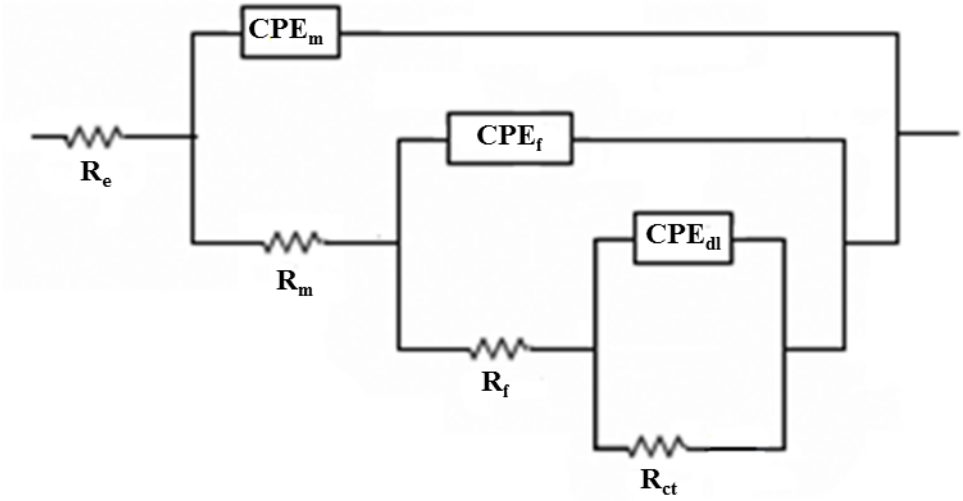

Fig. 6

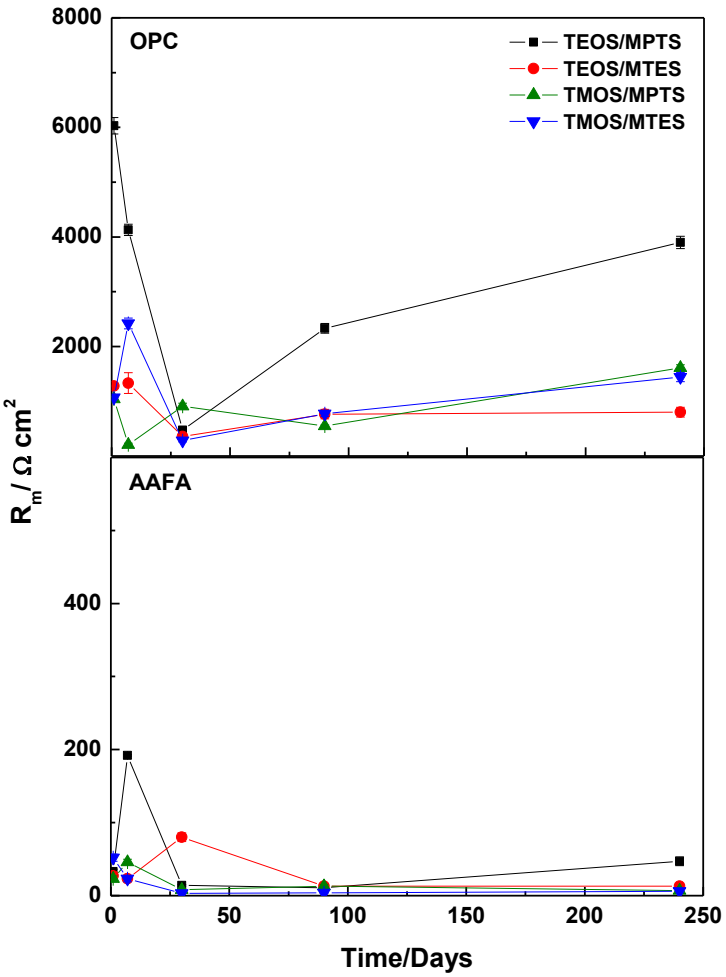
OPC
AAFA
TEOS/MPTS
TEOS/MTES
TMOS/MPTS
TMOS/MTES
R_m / Ω cm^2
Time/Days

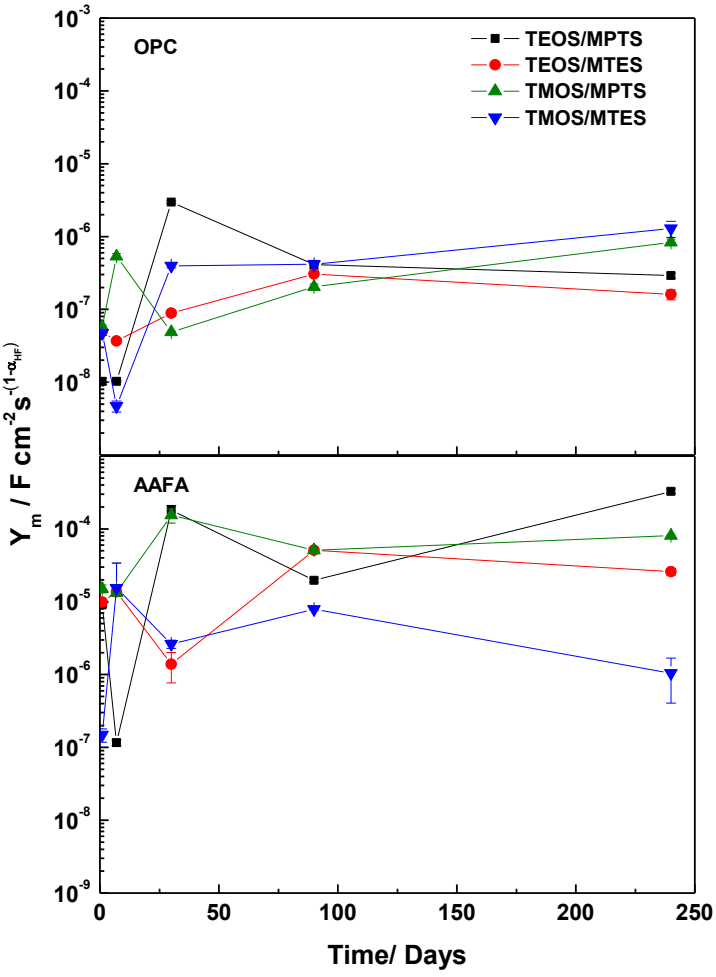
OPC
AAFA
TEOS/MPTS
TEOS/MTES
TMOS/MPTS
TMOS/MTES
Y_m / F cm^{-2} s$^{-(1-\alpha_{HF})}$
Time/ Days

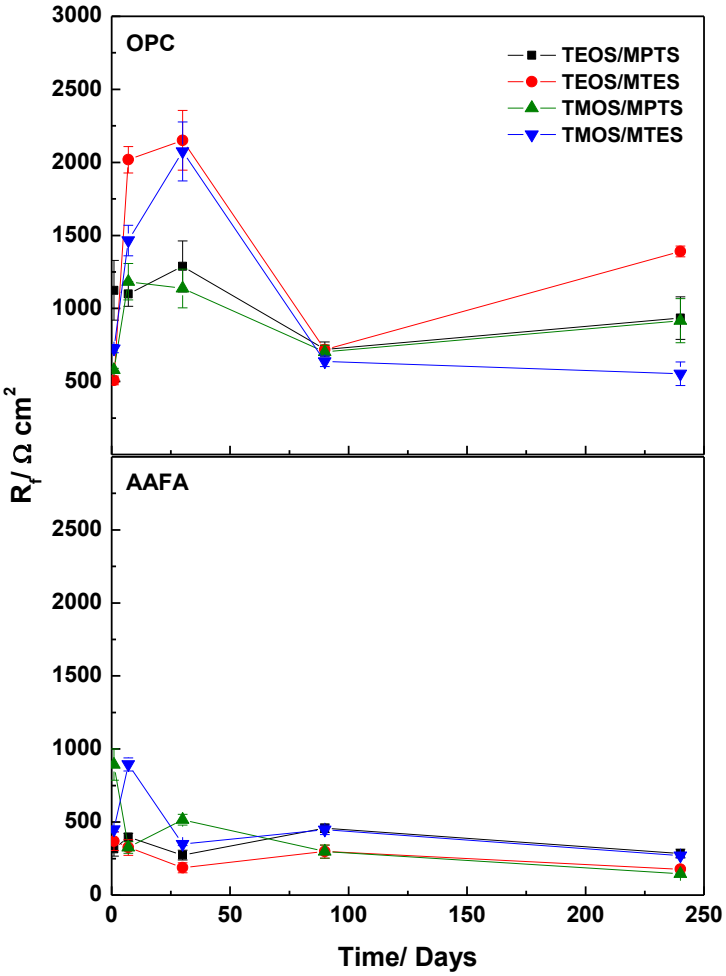
OPC
AAFA
TEOS/MPTS
TEOS/MTES
TMOS/MPTS
TMOS/MTES
R_f/ Ω cm^2
Time/ Days

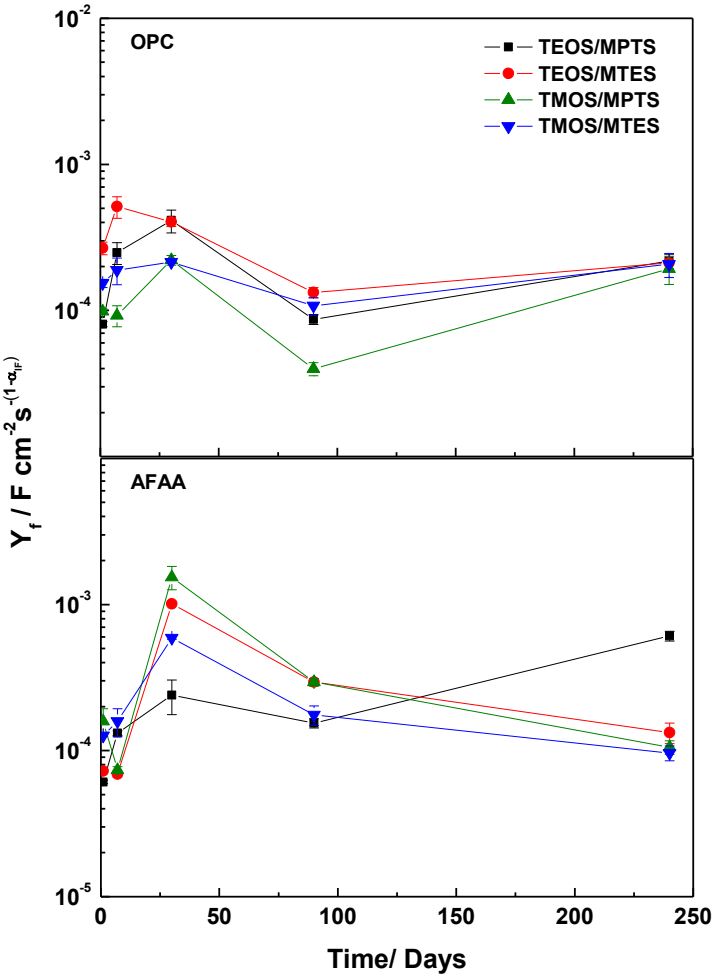
OPC
AFAA
TEOS/MPTS
TEOS/MTES
TMOS/MPTS
TMOS/MTES
Y_f / F cm^{-2}s$^{-(1-\alpha_{IF})}$
Time/ Days

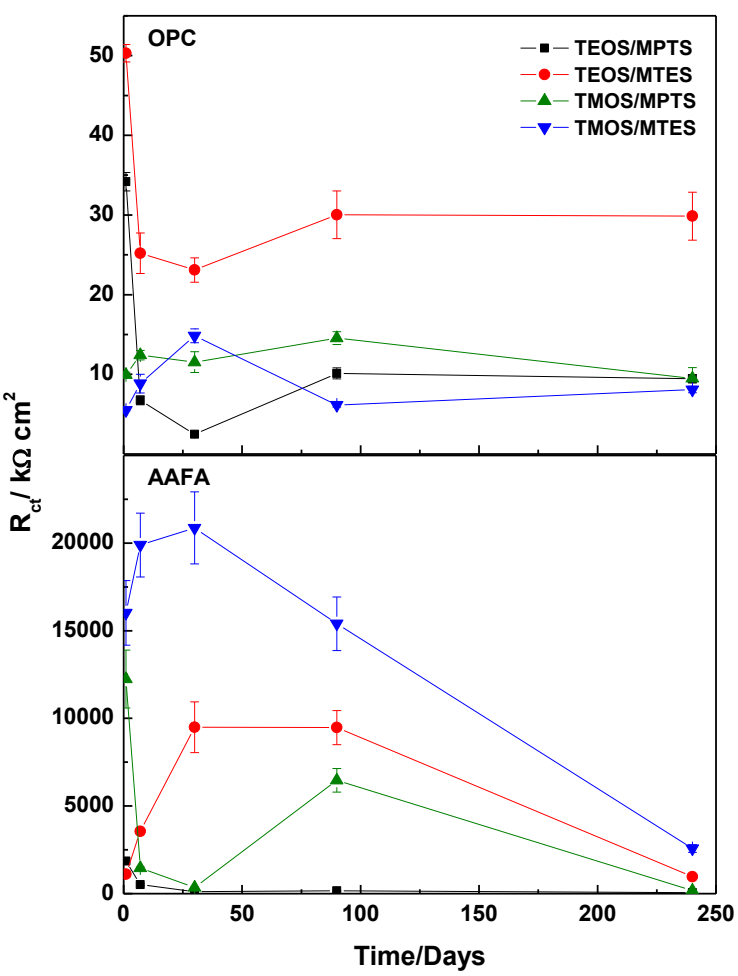
OPC
AAFA
TEOS/MPTS
TEOS/MTES
TMOS/MPTS
TMOS/MTES
R_ct / kΩ cm^2
Time/Days

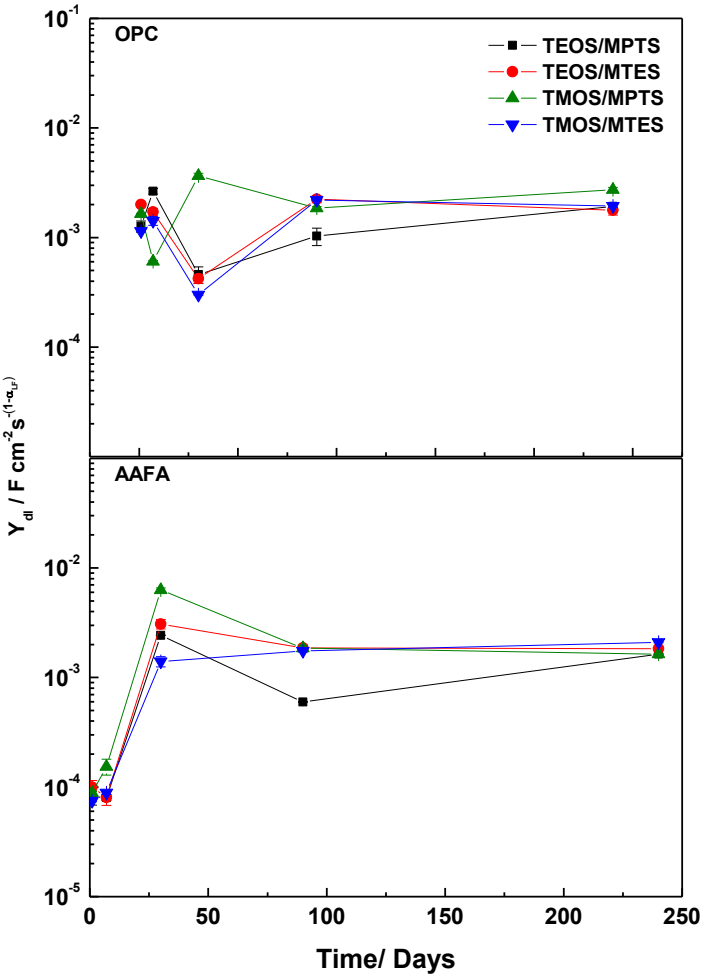
OPC
AAFA
TEOS/MPTS
TEOS/MTES
TMOS/MPTS
TMOS/MTES
Y_dl / F cm^-2 s^-(1-α_P)
Time/ Days

Table 1. Chemical composition (% in mass) and Blaine finesses of the tested ordinary Portland cement (OPC) and fly ash (FA).

	OPC	FA
LOI	3.28	6.76
IR	1.04	1.96
SiO_2	21.13	46.32
Al_2O_3	4.16	31.01
Fe_2O_3	3.80	4.50
CaO	63.94	4.90
MnO	0.01	0.05
Na_2O	0.25	0.34
K_2O	0.74	1.34
MgO	0.13	1.29
SO_3	3.06	0.91
Si_{react}	–	36.4
Free CaO	1.28	–
Blaine (m^2 kg^{-1})	386.7	336

LOI=Loss on Ignition, IR=Insoluble Residue

Table 2. Hardening (Step I and Step II), carbonation (Step III) and exposure steps for reinforced mortar specimens. During Step IV carbon steel reinforced specimens were partially immersed in a 3 wt.% NaCl solution.

Step	OPC Mortar	AAFA Mortar
I	24 h at room temperature, 100% RH	24 h in oven at 85 ºC, 100% RH
II	28 days in a humidity chamber (98% RH, 20±2ºC)	
III	60 days in a carbonation chamber at a 43.2% RH in a K_2CO_3 solution. The chamber was CO_2 saturated by filling it with the gas two times a day [32]	
IV	240 days of partial immersion in a 3 wt.% NaCl solution	

Table 3. Parameters used in the fitting of impedance data for the carbonated OPC mortar with uncoated steel rebar after different times of immersion in a 3 wt.% NaCl solution. The error, in %, associated with each parameter value is given in parenthesis.

Time Day	R_e Ω cm^2	Y_m, nF cm^{-2} $s^{-(1-\alpha_{HF})}$	α_m	R_m Ω cm^2	Y_f, µF cm^{-2} $s^{-(1-\alpha_{IF})}$	α_f	R_f Ω cm^2	Y_{dl}, mF cm^{-2} $s^{-(1-\alpha_{LF})}$	α_{dl}	R_{ct} KΩ cm^2
1	0	61 (9)	0.64 (1)	1251 (6)	480 (8)	0.50 (3)	662 (6)	5 (7)	0.65 (5)	3 (13)
7	0	64 (12)	0.62 (1)	2161 (1)	91 (13)	0.71 (4)	659 (6)	2 (5)	0.53 (5)	13 (15)
30	1910 (1)	1061 (13)	0.55 (3)	770 (4)	121 (10)	0.65 (3)	318 (5)	3 (1)	0.56 (2)	22 (13)
90	2617 (1)	602 (20)	0.76 (8)	416 (8)	142 (11)	0.62 (5)	1269 (7)	3 (13)	0.67 (7)	4 (17)
240	3350 (1)	370 (8)	0.58 (2)	1863 (2)	67 (6)	0.65 (2)	594 (3)	2 (1)	0.70 (3)	5 (8)

Table 4. Parameters used in the fitting of impedance data for the carbonated AAFA mortar with uncoated steel rebar after different times of immersion in a 3 wt.% NaCl solution. The error, in %, associated with each parameter value is given in parenthesis.

Time Day	R_e Ω cm^2	Y_m, µF cm^{-2} $s^{-(1-\alpha_{HF})}$	α_m	R_m Ω cm^2	Y_f, µF cm^{-2} $s^{-(1-\alpha_{IF})}$	α_f	R_f Ω cm^2	Y_{dl} µF cm^{-2} $s^{-(1-\alpha_{LF})}$	α_{dl}	R_{ct} kΩ cm^2
1	347 (1)	10 (9)	0.78 (12)	56 (17)	59 (7)	0.86 (8)	550 (16)	63 (13)	0.85 (5)	3334 (17)
7	282 (1)	19 (13)	0.69 (18)	41 (14)	128 (12)	0.76 (13)	332 (13)	110 (17)	0.76 (9)	700 (12)
30	110 (2)	36 (13)	0.63 (11)	28 (18)	249 (12)	0.66 (7)	264 (17)	562 (11)	0.71 (3)	909 (15)
90	200 (2)	4 (9)	0.55 (12)	106 (4)	85 (19)	0.68 (4)	286 (7)	633 (2)	0.60 (1)	2630 (13)
240	250 (1)	1 (18)	0.57 (5)	163 (2)	148 (17)	0.60 (4)	211 (9)	513 (9)	0.66 (4)	2 (16)

Table 5. Parameters used in the fitting of impedance data for the carbonated OPC mortar with coated steel rebar after different times of immersion in a 3 wt.% NaCl solution. The error, in %, associated with each parameter value is given in parenthesis.

Time Day	R_e Ω cm^2	Y_m, nF cm^{-2} $s^{-(1-\alpha_{HF})}$	α_m	R_m Ω cm^2	Y_f, µF cm^{-2} $s^{-(1-\alpha_{IF})}$	α_f	R_f Ω cm^2	Y_{dl}, mF cm^{-2} $s^{-(1-\alpha_{LF})}$	α_{dl}	R_{ct} KΩ cm^2
TEOS/MPTS										
1	0	10 (10)	0.72 (1)	6030 (6)	80 (12)	0.62 (11)	1124 (18)	1 (12)	0.55 (12)	34 (16)
7	0	10 (3)	0.78 (1)	4130 (1)	250 (17)	0.49 (6)	1099 (9)	3 (6)	0.58 (7)	7 (18)
30	3472 (1)	2965 (18)	0.63 (6)	475 (4)	413 (18)	0.45 (7)	1288 (17)	5 (18)	0.92 (17)	2 (12)
90	5469 (1)	413 (13)	0.61 (2)	2331 (8)	87 (19)	0.64 (19)	720 (18)	1 (18)	0.41 (19)	10 (17)
240	5543 (1)	291 (8)	0.54 (1)	3901 (2)	218 (18)	0.49 (13)	934 (16)	2 (6)	0.61 (3)	9 (18)
TEOS/MTES										
1	628 (2)	49 (6)	0.77 (1)	1276 (1)	267 (10)	0.58 (4)	507 (6)	2 (1)	0.58 (2)	50 (18)
7	873 (12)	64 (15)	0.79 (8)	1330 (14)	514 (17)	0.38 (14)	2018 (6)	2 (18)	0.83 (10)	25 (10)
30	3404 (1)	89 (19)	0.92 (9)	357 (14)	403 (17)	0.43 (10)	2151 (16)	0.4 (11)	0.59 (10)	23 (16)
90	3855 (1)	306 (14)	0.69 (2)	764 (8)	133 (8)	0.48 (4)	718 (4)	2 (13)	0.68 (7)	30 (17)
240	4043 (1)	160 (15)	0.71 (2)	801 (2)	211 (3)	0.41 (2)	1390 (3)	2 (1)	0.72 (3)	30 (19)
TMOS/MPTS										
1	228 (14)	58 (6)	0.71 (1)	1039 (3)	98 (4)	0.75 (1)	580 (2)	2 (1)	0.60 (1)	10 (3)
7	2066 (1)	535 (11)	0.84 (9)	208 (12)	92 (16)	0.67 (5)	1183 (10)	0.6 (2)	0.61 (2)	12 (5)
30	3729(1)	49 (11)	0.81 (4)	909 (6)	221 (8)	0.48 (2)	1137 (5)	4 (5)	0.68 (4)	11 (18)
90	4323 (1)	205 (9)	0.79 (8)	550 (3)	40 (12)	0.64 (6)	702 (6)	2 (3)	0.62 (4)	14 (14)
240	4972 (1)	834 (10)	0.56 (2)	1608 (4)	193 (11)	0.48 (17)	917 (16)	3 (5)	0.60 (3)	9 (18)
TMOS/MTES										
1	421 (6)	47 (8)	0.75 (1)	1067 (2)	153 (6)	0.67 (2)	725 (4)	1 (1)	0.63 (1)	5 (2)
7	0	5 (17)	0.85 (2)	2419 (1)	190 (11)	0.55 (7)	1465 (14)	1 (9)	0.76 (7)	8 (13)
30	2366 (1)	396 (14)	0.82 (8)	280 (8)	214 (1)	0.57 (1)	2075 (5)	0.3 (1)	0.49 (3)	15 (6)
90	2778 (1)	416 (13)	0.66 (7)	774 (7)	107 (13)	0.62 (5)	638 (6)	2 (2)	0.71 (2)	6 (4)
240	2922 (1)	1295 (15)	0.52 (5)	1442 (6)	207 (19)	0.51 (11)	553 (15)	2 (3)	0.70 (2)	8 (5)

Table 6. Parameters used in the fitting of impedance data for the carbonated AAFA mortar with coated steel rebar after different times of immersion in a 3 wt.% NaCl solution. The error, in %, associated with each parameter value is given in parenthesis.

Time Day	R_e Ω cm^2	Y_m, µF cm^{-2} $s^{-(1-\alpha_{HF})}$	α_m	R_m Ω cm^2	Y_f, µF cm^{-2} $s^{-(1-\alpha_{IF})}$	α_f	R_f Ω cm^2	Y_{dl} µF cm^{-2} $s^{-(1-\alpha_{LF})}$	α_{dl}	R_{ct} kΩ cm^2
TEOS/MPTS										
1	201 (1)	9 (15)	0.73 (7)	33 (8)	61 (17)	0.86 (4)	316 (16)	80 (15)	0.89 (2)	1853 (14)
7	0	0.1 (12)	0.74 (2)	192 (1)	132 (4)	0.76 (1)	396 (7)	80 (6)	0.91 (1)	517 (11)
30	228 (1)	180 (16)	0.53 (2)	14 (10)	240 (16)	0.73 (5)	274 (16)	144 (16)	0.83 (5)	115 (15)
90	197 (1)	20 (14)	0.73 (2)	11 (15)	154 (7)	0.63 (1)	458 (6)	93 (6)	0.83 (1)	161 (6)
240	182 (1)	328 (7)	0.50 (3)	48 (16)	6 (16)	0.99 (8)	284 (11)	165 (12)	0.77 (2)	62 (11)
TEOS/MTES										
1	201 (1)	9 (13)	0.80 (15)	27 (19)	72 (12)	0.85 (5)	369 (17)	101 (15)	0.87 (2)	1113 (16)
7	200 (1)	14 (14)	0.78 (16)	23 (15)	69 (12)	0.84 (6)	326 (16)	80 (15)	0.89 (2)	648 (9)
30	46 (9)	1 (14)	0.75 (6)	80 (7)	1010 (14)	0.62 (8)	187 (19)	3086 (10)	0.73 (4)	9491 (16)
90	135 (13)	51 (14)	0.57 (15)	13 (8)	294 (5)	0.57 (7)	298 (15)	1864 (5)	0.69 (7)	9472 (11)
240	174 (1)	26 (15)	0.67 (3)	13 (14)	134 (16)	0.60 (4)	178 (5)	1834 (1)	0.62 (3)	270 (15)
TMOS/MPTS										
1	153 (1)	15 (13)	0.70 (17)	23 (19)	159 (12)	0.74 (4)	894 (17)	89 (18)	0.72 (4)	12241 (18)
7	319 (1)	13 (15)	0.75 (19)	46 (13)	74 (13)	0.81 (9)	326 (11)	154 (16)	0.83 (3)	1464 (16)
30	90 (12)	154 (11)	0.59 (19)	8 (6)	1537 (18)	0.56 (17)	516 (15)	6311 (12)	0.80 (11)	344 (17)
90	135 (13)	51 (9)	0.57 (18)	13 (17)	294 (16)	0.57 (15)	298 (15)	1864 (6)	0.69 (4)	9472 (10)
240	139 (1)	1 (14)	1.00 (16)	7 (18)	105 (11)	0.70 (2)	146 (3)	1640 (5)	0.59 (3)	1816 (12)
TMOS/MTES										
1	120 (4)	0.1 (18)	0.86 (12)	52 (9)	127 (1)	0.73 (1)	449 (3)	75 (2)	0.82 (1)	16021 (12)
7	153 (1)	15 (12)	0.70 (17)	23 (19)	159 (16)	0.74 (4)	895 (16)	88 (18)	0.72 (4)	19889 (16)
30	97 (2)	3 (13)	1.00 (8)	3 (10)	591 (12)	0.58 (7)	350 (12)	1401 (11)	0.66 (5)	20864 (13)
90	139 (1)	7 (13)	0.80 (12)	4 (13)	175 (15)	0.61 (4)	447 (7)	1749 (2)	0.61 (3)	15397 (16)
240	141 (1)	1 (11)	1.00 (5)	6 (17)	96 (12)	0.68 (3)	270 (5)	2096 (1)	0.53 (3)	2576 (15)